



UNIVERSITY OF LEEDS

This is a repository copy of *Experimental Investigation of Oil Recovery Performance and Permeability Damage in Multilayer Reservoirs after CO₂ and Water–Alternating-CO₂ (CO₂–WAG) Flooding at Miscible Pressures*.

White Rose Research Online URL for this paper:
<http://eprints.whiterose.ac.uk/156719/>

Version: Accepted Version

Article:

Wang, Q, Yang, S, Lorinczi, P et al. (2 more authors) (2020) Experimental Investigation of Oil Recovery Performance and Permeability Damage in Multilayer Reservoirs after CO₂ and Water–Alternating-CO₂ (CO₂–WAG) Flooding at Miscible Pressures. *Energy & Fuels*, 34 (1). pp. 624-636. ISSN 0887-0624

<https://doi.org/10.1021/acs.energyfuels.9b02786>

© 2019 American Chemical Society. This is an author produced version of an article published in *Energy and Fuels*. Uploaded in accordance with the publisher's self-archiving policy.

Reuse

Items deposited in White Rose Research Online are protected by copyright, with all rights reserved unless indicated otherwise. They may be downloaded and/or printed for private study, or other acts as permitted by national copyright laws. The publisher or other rights holders may allow further reproduction and re-use of the full text version. This is indicated by the licence information on the White Rose Research Online record for the item.

Takedown

If you consider content in White Rose Research Online to be in breach of UK law, please notify us by emailing eprints@whiterose.ac.uk including the URL of the record and the reason for the withdrawal request.



eprints@whiterose.ac.uk
<https://eprints.whiterose.ac.uk/>

Experimental investigation of oil recovery performance and permeability damage in multilayer reservoirs after CO₂ and Water-Alternating-CO₂ (CO₂-WAG) flooding at miscible pressures

Qian Wang^{1,2}, Shenglai Yang^{1*}, Piroska Lorinczi², Paul W.J. Glover², Hao Lei³

1 School of Petroleum Engineering, China University of Petroleum-Beijing, Beijing 102249, China

2 School of Earth and Environment, University of Leeds, Leeds, LS2 9JT, UK

3 Research Institute of Exploration and Development, Sinopec Jiangnan Oilfield Company, Wuhan, 430223, China

* Correspondence: yshenglai820@163.com

Abstract: Blockage in reservoirs caused by asphaltene deposits and inorganic interactions is a serious problem that may exacerbate the complexity of displacement characteristics in heterogeneous multilayer sandstone reservoirs and affect crude oil recovery performance during CO₂ and CO₂-WAG flooding. In this study, experiments of both CO₂ and CO₂-WAG flooding were carried out on the same multilayer systems under miscible conditions (70°C, 18 MPa). The two flooding methods were evaluated for oil production performance and reservoir damage. The experimental results indicate that, after CO₂ flooding, the entire system has a low oil recovery factor (RF) of 27.6%, and oil is produced mainly from the high permeability layer (91.4%), whilst the residual oil remains predominantly in the medium and low permeability layers. The injection pressure of CO₂-WAG flooding is high, but the timing of CO₂ breakthrough (BT) is late, and the oil RF of the entire system reaches 44.5%. The contribution rate of oil production in medium and low permeability layers is improved to 3.8% and 17.1%, respectively. Furthermore, the permeability of the high permeability layer decreases by 16.8% after CO₂ flooding, which is mainly due to asphaltene precipitation. However, after CO₂-WAG flooding, the permeability of each layer is significantly reduced, namely by 29.4%, 16.8% and 6.9% respectively. Asphaltene precipitation is still the main factor, but permeability decline caused by CO₂-brine-rock interactions cannot be ignored, especially in the high permeability layer (6.1%). Therefore, for multilayer reservoirs with high heterogeneity, CO₂-WAG flooding provides the better oil displacement performance, but prevention and control measures for asphaltene precipitation are more necessary.

Keywords: CO₂ and CO₂-WAG flooding, residual oil distribution, permeability decline, asphaltene precipitation, CO₂-brine-rock interactions, multilayer heterogeneous reservoir, core-flooding

Introduction

The injection of CO₂ into reservoirs is a reliable form of enhanced oil recovery (EOR) ^[1-4]. Oil viscosity reduction as a result of CO₂ dissolution can improve the fluidity of crude oil effectively and increase oil displacement efficiency, while the effects of interfacial tension (IFT) reduction, light-hydrocarbon extraction, and oil-swelling also contribute to enhanced oil recovery ^[5-8]. Moreover, above the minimum miscible pressure (MMP), CO₂ and oil can mix together in any proportion and create a single phase. Consequently, oil recovery factor (RF) is further improved by eliminating or reducing IFT through multiple contacts of CO₂ and oil in reservoirs ^[9-12].

Flooding with both CO₂ and CO₂-WAG are common EOR strategies which have been widely used in a significant number of oilfields ^[13-15]. Each flooding scheme has individual characteristics in terms of displacement effect, injection difficulty, and impact on the reservoir's physical properties ^[16-19]. Since CO₂ has a lower viscosity and density at reservoir conditions, the pressure required for CO₂ injection during CO₂ flooding is small. However, the lower density of CO₂ promotes viscous fingering and gravity segregation which leads to early CO₂ breakthrough (BT), low CO₂ utilization efficiency and low oil RFs ^[20-21]. This is especially the case when the actual oil-bearing reservoir consists of a series of thin layers with different permeabilities separated by restraining barriers. In this case, CO₂ breakthrough occurs prematurely in high permeability layers due to the smaller resistive capillary force, and resulting in a large amount of crude oil remaining in the layers with lower permeability ^[22]. Flooding with a CO₂-WAG scheme can enlarge sweep volume of injected fluid to improve the effective amount of injected CO₂, reducing the impact of heterogeneity between layers. However, the combination of high injection pressures and the complex operation of switching between CO₂ injection and water injection increases the cost of injection, which is a disadvantage of CO₂-WAG flooding in low permeability and tight reservoirs ^[18-19].

In addition, when CO₂ is in contact with fluids and rocks in reservoirs during the injection process, the processes of organic (i.e., asphaltene) and inorganic (i.e., metal carbonate) precipitation are triggered ^[23-24]. When the pressure reaches a certain value in the CO₂ injection process, changes in composition of the crude oil due to the dissolved CO₂ lead to asphaltene precipitation. The asphaltene solid particles are captured or adsorbed on the pores' walls, resulting in blocked pores and pore throats ^[25-28]. Moreover, variations of ion concentration and the pH of the brine caused by CO₂-brine-rock interactions lead to precipitation of metal carbonates. In addition, the dissolution of clay minerals leads to the release of clay particles. Both of these inorganic processes can also cause pore throats to be blocked ^[29-31]. The above mentioned precipitation and blockage, especially for rocks with low permeability, which have smaller pore-throat structure, cause greater damage to the reservoirs, usually resulting in a decrease of permeability, affecting the flow of fluid in the reservoir, and reducing the effect of CO₂-EOR^[23].

Furthermore, the distribution of fluids in rocks with different pore size distributions during the flooding process can vary greatly due to the heterogeneity of permeability between the thin layers [22,32]. Crude oil, water and CO₂ are all affected, but CO₂ is particularly affected because the concentration of CO₂ is one of the key factors for CO₂–oil–brine–rock interactions. Different flooding schemes can also increase this variation [30,33], which makes predicting damage to reservoirs and residual distribution more difficult, and as such these are also a focus of concern for oilfields. Consequently, the oil recovery performance, residual oil distribution and changes in physical properties in multilayer reservoirs undergoing different flooding schemes are worthy of further study.

A large number of previous experiments have compared the effect of different CO₂ flooding schemes on EOR and the residual oil [33-37], while others have studied asphaltene precipitation after different CO₂ flooding schemes under different experimental conditions [38-42]. However, the mutual relationship between oil recovery, residual oil and permeability decline has rarely been studied in multilayer reservoirs for different flooding methods. The combined effect and difference between asphaltene precipitation and CO₂–brine–rock interactions on damage to pore structure have been ignored in most past studies [26, 28, 38-42]. Unfortunately rock cores cannot be reused in multiple experiments under different conditions due to irreversible changes caused predominantly by CO₂–brine–rock interactions in rocks during flooding processes [43-44]. Previous studies using ‘matched’ initial core material used in comparative experiments have often been unsatisfactory.

In this work, the oil recovery, residual oil and reservoir damage has been measured during CO₂ and CO₂-WAG flooding of model heterogeneous multilayer sandstone reservoirs with variable permeability under miscible conditions. The MMP of the CO₂–crude oil system was measured by applying an IFT test apparatus. Two groups of cores with similar physical properties were obtained by dividing three cores, and were used to simulate multilayer reservoirs. Full CO₂ and CO₂-WAG core-flooding experiments were conducted on the multilayer systems at reservoir temperature (70±7°C) and pressure (18±1.5 MPa, >MMP). The post-flood oil RF, residual oil distribution and damage of inorganic and organic precipitation to permeability of each core in the multilayer systems were evaluated for each of the two flooding schemes. The different performances of the two flooding schemes have been analysed and discussed in detail based on the experimental results.

Methodology

Materials

In this study, crude oil was collected from Changqing Oilfield, which is located in the Ordos Basin in western China (38°30′09″N, 108°50′37″E). The reservoir lies at a depth of 2100-2400 m and consists predominantly of low permeability sandstone. The crude oil used in the experiment was synthetic live oil (Table 1) that was prepared in the laboratory to match the composition of the produced oil. The composition of the crude oil was measured by using a high-temperature gas chromatograph apparatus

(Table 2). The content of *n*-C5 insoluble asphaltene of the crude oil was measured to be 1.32 wt% by using the standard ASTM D2007-03 method. In addition, the pressure at which asphaltene begins to precipitate in crude oil is 9.6 MPa at reservoir conditions, and the predicted relationship curves between asphaltene precipitation and the concentration of dissolved CO₂ in crude oil, based on the Flory-Huggins model, is shown in Figure 1^[24].

The formation water used in experiments was prepared according to the composition given in Table 3. The brine was considered to consist predominantly of dissolved calcium chloride with a total dissolved solids (TDS) of 29520 mg/dm³. Ordinary distilled water and deuterium oxide were used to prepare two types of brine, ordinary brine and deuterium oxide brine. The purity of the CO₂ used in this study was 99.99%, the solubility of CO₂ in the crude oil is 58.7 mol% at 18 MPa and 70°C.

Table 1. Basic physical properties of live oil.

Items	Live oil
Density (g/cm ³)	0.725±0.002 (70°C)
Viscosity (cP)	3.88±0.05 (70°C)
DGOR (m ³ /m ³)	31.4
Bubble point pressure (MPa)	7.52

Table 2. Compositional analysis result of the live oil (*n*-C5 insoluble asphaltene content =1.32 wt%).

Carbon number	wt%	Carbon number	wt%	Carbon number	wt%
CO2	0.08	C9	6.46	C21	1.80
N2	0.31	C10	5.70	C22	1.92
C1	1.50	C11	4.86	C23	1.67
C2	0.60	C12	4.21	C24	1.74
C3	0.49	C13	4.28	C25	1.59
iC4	0.25	C14	4.45	C26	1.56
nC4	0.47	C15	3.88	C27	1.58
iC5	1.18	C16	3.38	C28	1.48
nC5	0.22	C17	3.08	C29	1.40
C6	4.86	C18	2.93	C30+	15.78
C7	5.55	C19	2.38	Total	100
C8	6.10	C20	2.28		

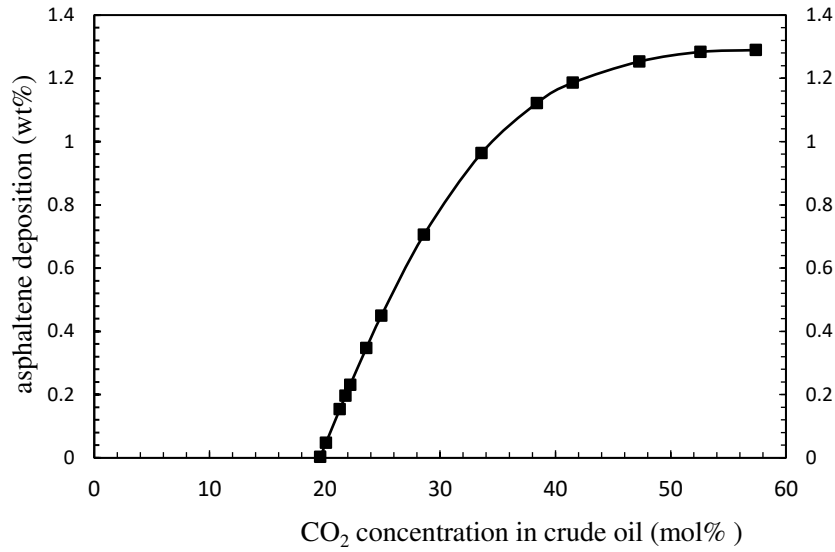


Figure 1. Effect of CO₂ on the amount of asphaltene deposition (wt%) at $P=18$ MPa and $T=70$ °C

Table 3. Physicochemical properties of the reservoir brine.

Item	Value
Density (g/cm ³)	1.01
Viscosity at 25°C (cP)	1.03
pH	7.04
K ⁺ (mg/L)	296
Na ⁺ (mg/L)	3494
Ca ²⁺ (mg/L)	7134
Mg ²⁺ (mg/L)	48.2
Cl ⁻ (mg/L)	18433
SO ₄ ²⁻ (mg/L)	114
TDS(mg/L)	29520

The core samples, numbered Y-1, Y-2, and Y-3 were taken from different thin production layers of the reservoir which had not been subjected to previous CO₂-EOR operations. These cores are homogeneous sandstones and have different permeabilities, representing the average permeability of each layer. The cores were cleaned to remove organic and inorganic fluids and were measured to obtain porosity and permeability values by the high-pressure helium permeameter-porosimeter (TEMCO, Inc. Tulsa, OK, USA) after being dried, obtaining the average value of three measurements (uncertainties < 0.3%). After that, each core was divided into two sections to obtain six cores of two groups, all with same length (Figure 2, Table 4).

The mineral components (Table 5) of the cores were measured by X-ray diffraction (XRD, Model: D8 Focus, Bruker, MA, USA). All cores were completely saturated with ordinary brine under vacuum for 24 hours and were measured by NMR apparatus (Mini-MR, Niumag, China). The magnetic intensity, gradient value control precision, and frequency range of the NMR apparatus were 0.5 T, 0.025 T/m, 0.01 MHz, and 1–30 MHz, respectively. During the NMR tests, the transverse relaxation time (T_2) and

magnetization of the hydrogen nuclei of the ordinary brine in all core pores were recorded to obtain the T_2 spectra. Since the T_2 value and corresponding signal amplitude represented the size and amount of pore space in which the hydrogen nuclei were located, the T_2 spectra were converted into the pore size distribution of the cores ^[45] (Figure 6).

Petrophysical test results have demonstrated that the two short cores from the same divided core have almost the same permeability, porosity and pore size distribution, which is considered to satisfy the premise of the same physical properties of the experimental materials before the experiments.

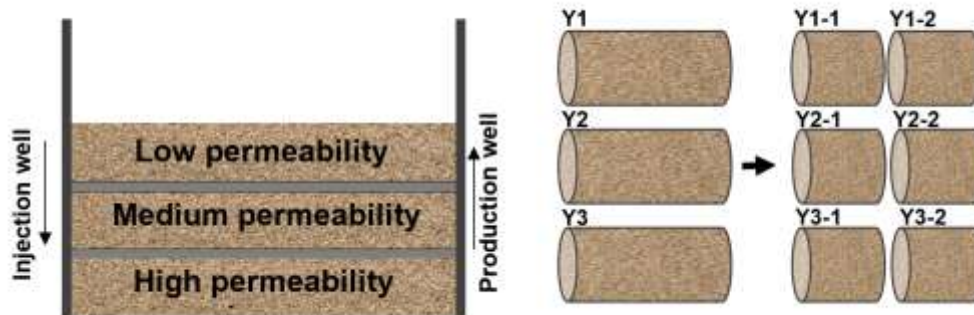


Figure 2. Schematic of multilayer reservoir and core segmentation.

Table 4. Basic parameters of the core samples.

Core number	Length (cm)	Permeability (mD)	Porosity (%)	Diameter (cm)
Y1	6.75	0.589	10.67	2.523
Y1-1	3.15	0.582	10.61	2.523
Y1-2	3.12	0.593	10.68	2.523
Y2	6.58	6.82	16.74	2.525
Y2-1	3.1	6.78	16.69	2.525
Y2-2	3.13	6.92	16.87	2.525
Y3	6.84	63.2	19.91	2.522
Y3-1	3.14	63.6	19.98	2.522
Y3-2	3.13	64.1	19.85	2.522

Table 5. Types and contents of mineral in the cores.

Core number	Mineral types and content (wt. %)						
	Quartz	K-feldspar	Plagioclase	Calcite	Dolomite	Clay minerals	Others
Y1	33.5	16.3	31.2	6.5	2.2	6.8	3.5
Y2	41.3	13.4	26.6	7.7	2.8	5.4	2.8
Y3	30.4	18.5	36.2	5.1	1.8	4.9	3.1

The MMP Test

In this study, the MMP of the crude oil–CO₂ system was measured by using the vanishing interfacial tension (VIT) technique developed as an IFT-based experimental method^[9-10] (Figure 3). In this method, the equilibrium IFTs between the crude oil and CO₂ are measured accurately at various equilibrium pressures and at the reservoir temperature by applying the axisymmetric drop shape analysis (ADSA) technique for the pendant drop case. Subsequently, the MMP of the crude oil–CO₂ system is obtained by linearly extrapolating the measured equilibrium IFT and pressure data to zero IFT.

The apparatus comprises a high-pressure IFT cell (IFT-10, Temco, Fremont, CA, USA) with a maximum operating pressure and temperature of 69 MPa and 177°C, respectively. After heating the setup to the temperature of 70°C, CO₂ was pumped into the optical cell to the designated pressure and the crude oil was injected into the optical cell to form oil droplets through a stainless steel syringe needle by a pump (260D, ISCO, Lincoln, NE, USA). The pendant drop remained two minutes at the tip of the syringe needle before dropping off when equilibrium was achieved. A microscope camera was used to capture a series of digital images of the oil pendants at different times and the shapes of the oil pendants were analyzed by software (FTA, First Ten Angstroms Portsmouth, VA, USA) based on ADSA to measure the dynamic IFT of oil drop and the CO₂ phase. The IFT tests at different designated pressures were repeated three times and the measurement errors between different tests were less than ± 0.5 mJ/m².

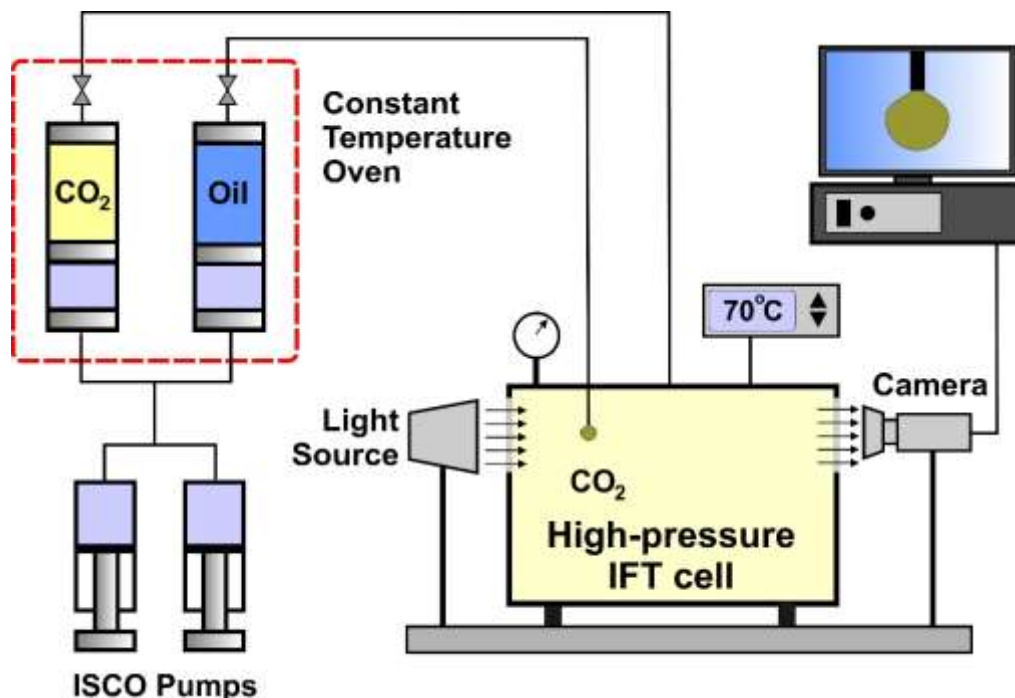


Figure 3. Schematic diagram of the apparatus used to measure the equilibrium IFT between CO₂ and crude oil at reservoir conditions.

The results are shown in Figure 4. The measured MMP value of the crude oil–CO₂ system is 16.8±0.3 MPa, indicating that the experimental pressure satisfied the minimum miscibility condition of crude oil and CO₂.

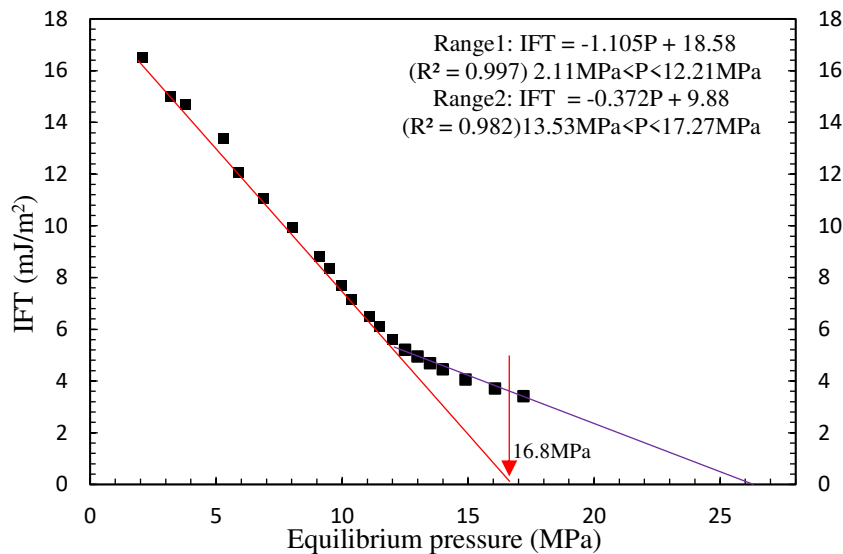


Figure 4. The measured IFT of the CO₂-crude oil system at different equilibrium pressures at a reservoir condition temperature of 70°C.

Core-flooding tests

Figure 5 shows the schematic diagram of the multilayer and high-pressure core flooding apparatus used for CO₂ and CO₂-WAG flooding experiments in this study. Three core holders (Hongda, China; $P=80$ MPa; $T=130^{\circ}\text{C}$) were connected in parallel and positioned horizontally to simulate the multilayer reservoir. Deuterium oxide brine, live oil, and CO₂ were contained separately in three tanks. All core holders and tanks were placed in the constant temperature oven (Hongda, China; $T=150.0\pm 0.1^{\circ}\text{C}$) with the temperature being regulated to within $\pm 0.1^{\circ}\text{C}$ by a three-term temperature controller.

A dual ISCO syringe pump was used to displace brine, crude oil, and CO₂ into the multilayer core system. Another pump was used to maintain confining pressure, while a third pump and three back pressure valves were used together to maintain and regulate the back pressure. A set of measuring devices were used to quantify the produced fluids (i.e., brine, oil, and gas) for each core separately. These devices included three mass flow meters and three gas-liquid separators. Pressure and flow data during the experiments were collected and logged automatically by computer.

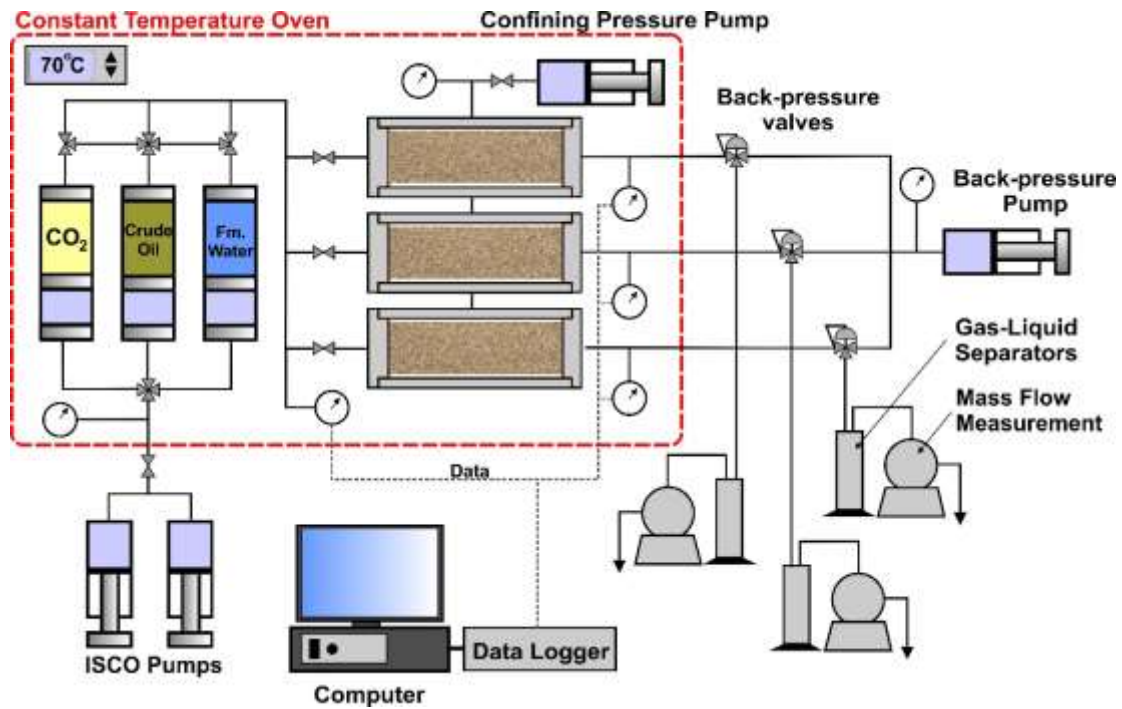


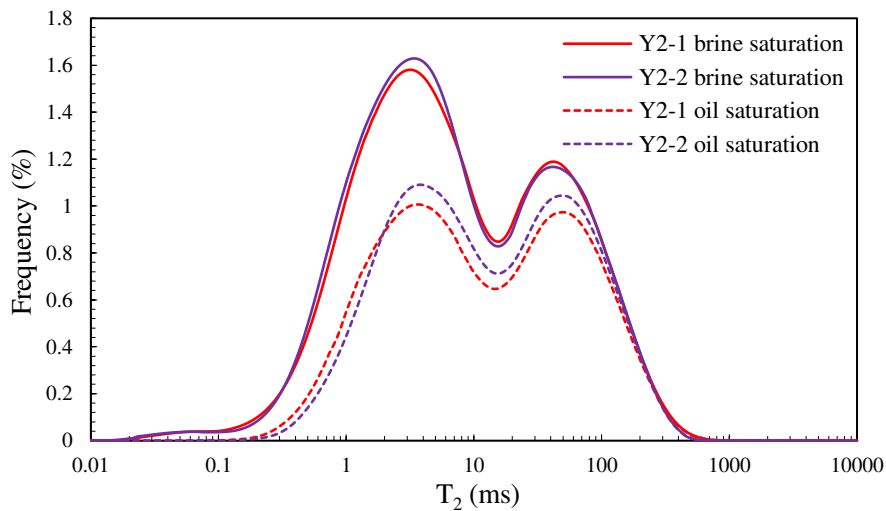
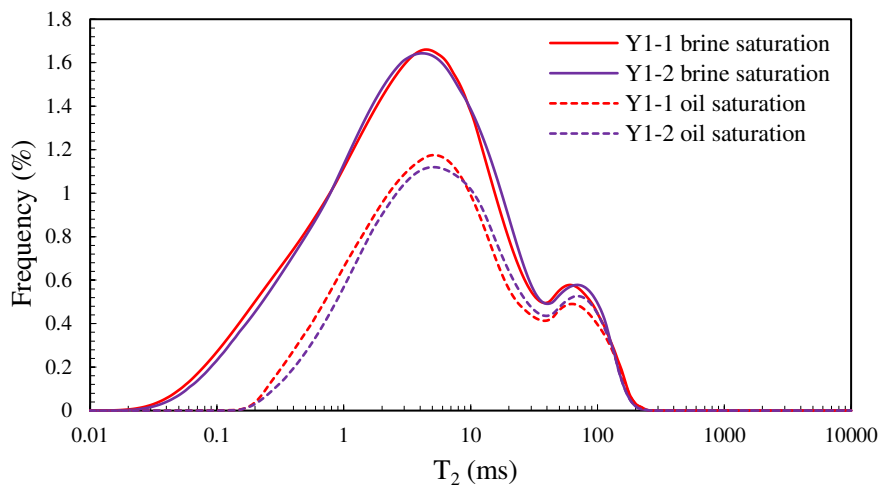
Figure 5. Schematic diagram of flooding experiments.

The general procedure of the core flooding tests can be described briefly as follows.

- (1) The constant temperature oven core system was set to 70°C and maintained for 24 hours to ensure that all parts in the constant temperature oven were heated to 70°C. The cores Y1-1, Y2-1, Y3-1 were placed in the core holders after being cleaned and dried again. Each core was then continuously evacuated separately for 24 hours, followed by injection of the deuterium oxide brine into the core separately. Thereafter, the crude oil was pumped into each core to achieve the initial oil saturation (S_{oi}) and the connate water saturation (S_{wc}) separately. The injection in each core was terminated after 30 HCPV of crude oil. After the continuous process of saturating the cores by oil, all core holders were left undisturbed for the whole day to attain a suitable equilibrium condition at the reservoir conditions.
- (2) A suite of NMR tests were carried out on each core. Since there were no hydrogen nuclei in the deuterium oxide brine, the measured NMR signal represents only those hydrogen nuclei in the crude oil, and consequently it is possible to obtain the distribution of the crude oil in each core (Figure 6, Table 6). All core holders were placed back in the constant temperature oven and left undisturbed for another 24 hours.
- (3) Both CO₂ and deuterium oxide brine were injected with a constant flow rate of 0.02 cm³/min in a typical WAG process. Injection was made into the multilayer system from the same inlet, and the fluid production from the three different layers was collected and measured separately. The pressure at the outlet of the core holders was controlled at 18 MPa using the back pressure pump and back pressure

valve. The WAG plug size was 0.10 HCPV and the WAG slug ratio was 1:1. The WAG coreflood was stopped when no more oil was produced from the multilayer system. The injection and production pressures were continuously monitored and recorded during the entire flooding, as well as the volume of injection and production fluid. The cores in the core holder were tested by NMR again to obtain the distribution of the residual oil in each core. In addition, the asphaltene content and components of oil produced were measured after experiments.

(4) The operation of (1)-(2) was conducted on the cores Y1-2, Y2-2, Y3-2, and CO₂ was injected into the cores with the same flow rate (i.e., 0.02 cm³/min) and the same outlet pressure. The injection was stopped when no more oil was produced and the volume of injection CO₂ reached the injection fluid volume of WAG flooding in Step (3). The distribution of the residual oil in each core was then measured using NMR once again.



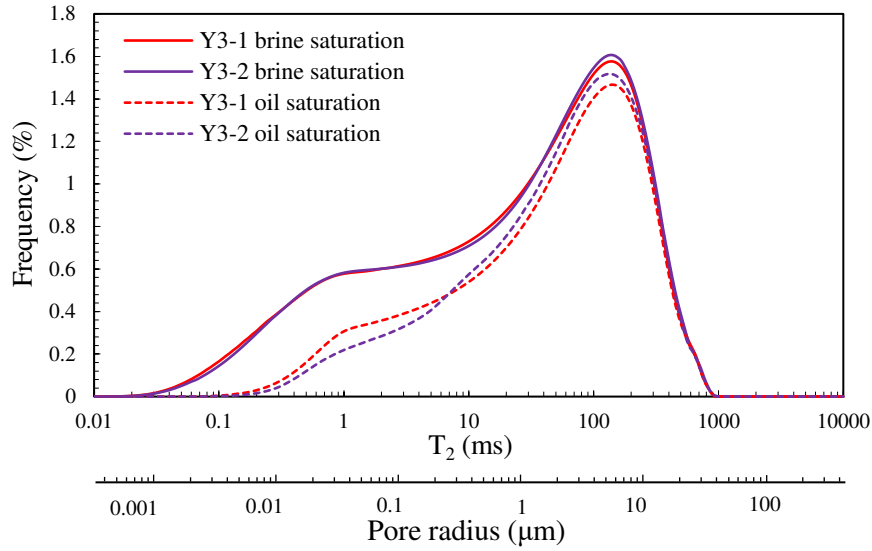


Figure 6. NMR T_2 spectrum of oil and brine distributions in cores before experiments.

Table 6. S_{oi} and S_{wc} in the core before the flooding experiment.

Core number	Pore volume (cm ³)	S_{oi} (%)	S_{wc} (%)	
Y1-1	1.67	62.3	37.7	CO ₂ -WAG flooding
Y2-1	2.59	67.1	32.9	
Y3-1	3.13	75.6	24.4	
Y1-2	1.67	60.2	39.8	CO ₂ flooding
Y2-2	2.64	69.8	30.2	
Y3-2	3.10	78.9	21.1	

Post-flooding tests

In order to obtain and distinguish the damage to petrophysical properties of cores caused by organic and inorganic interaction (CO₂–brine–rock interactions), an improved core cleaning method was used to clean the cores after experiments. Since the asphaltene is soluble in aromatics but not in alkanes, other components in the crude oil can be thoroughly mixed with *n*-heptane^[6,41], the cores were first cleaned by using a Soxhlet Extractor (SXT-02, Shanghai Pingxuan Scientific Instrument CO., Ltd., China) with *n*-heptane to remove the remaining fluid in the cores after flooding. Afterwards, the cores were dried and measured to obtain the gas permeability and porosity affected by the asphaltene precipitation and inorganic interactions together. Then the cores were cleaned with toluene + alcohol to remove the asphaltene, and then the cores were dried and were measured to obtain the porosity, permeability which were, at this stage, only affected by the inorganic interactions^[24], each value is the average of three measurements (uncertainties < 0.3%).

Results and Discussion

CO₂ and CO₂-WAG flooding results

Differential pressures

The differential pressures measured between the injection and production of the multilayer system during flooding are showed in Figure 7. During CO₂ flooding, the differential pressures increased at first and decreased subsequently, which is caused by the combined effects of the strong flow resistance of the two-phase flow at the beginning and the reduction of crude oil viscosity caused by CO₂ dissolution [6]. Obvious CO₂ breakthrough (BT) occurred in the high-permeability core. When there was no more crude oil produced, the differential pressures showed a slight upward trend. During CO₂-WAG flooding the differential pressures were higher than that during CO₂ flooding and the time of CO₂ BT in the core was later. These two effects were associated with the three-phase flow and relatively high viscosity of water. A higher injection pressure is required in CO₂-WAG flooding, but the CO₂ BT can be effectively delayed in multilayer systems.

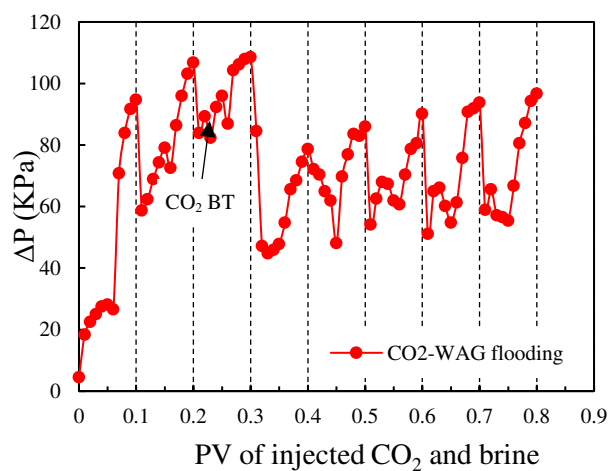
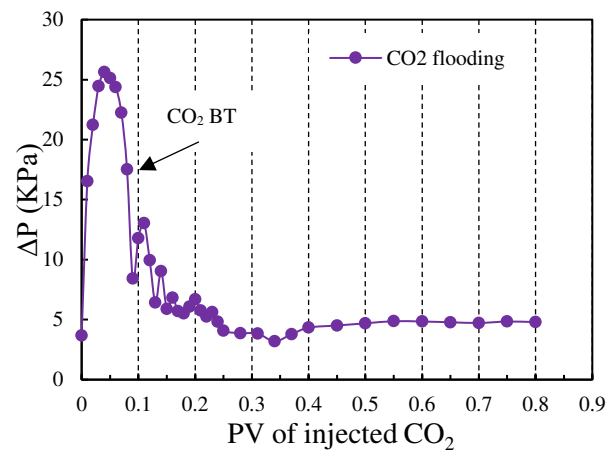


Figure 7. Measured differential pressure (ΔP) between the inlet and outlet of the multilayer system during flooding.

Produced fluid

Figure 8 and Table 7 show the cumulative gas production in the three cores and cumulative oil production in high permeability core during CO₂ flooding (the medium and low permeability cores had less fluid production and the volume cannot be accurately measured). During the initial stage, the gas production rate was low. As more CO₂ was injected, the gas production rate rose rapidly. When CO₂ BT occurred in this core, the produced gas flow fluctuated. This is because the gas produced in the early stage is mainly the dissolved gas in the crude oil; later the injected CO₂ is also discharged from the cores. However, the gas production rate in the middle permeability core was always low, and the cumulative gas production almost no longer increased after CO₂ BT. In the low permeability core almost no fluid production was observed. It indicates that little CO₂ entered the medium and low permeability cores. Therefore, the contribution of gas production in high-permeability cores decreased slowly and then rose, but was dominant during the flooding. The liquid produced by the multilayer system is almost entirely from the high permeability layer and the liquid produced is mainly oil.

Figure 9 and Table 7 show the cumulative gas and liquid (oil and brine) production in three cores during CO₂-WAG flooding. The values of cumulative gas production were so low for Y1 that they were below the noise threshold for the measurement devices, and have therefore been allocated a value of zero, the volume of liquid in the low permeability core cannot be accurately measured. Although the contribution rate of liquid and gas production of high permeability core was much higher than that of the other two cores, the medium permeability core still had obvious liquid and gas production, even after CO₂ BT in the high permeability core. Moreover, relatively obvious CO₂ BT had also occurred in the medium permeability core. The contribution rate of gas production in high-permeability cores decreased slowly and rose after CO₂ BT. Produced gas and oil droplets were observed in the low permeability core.

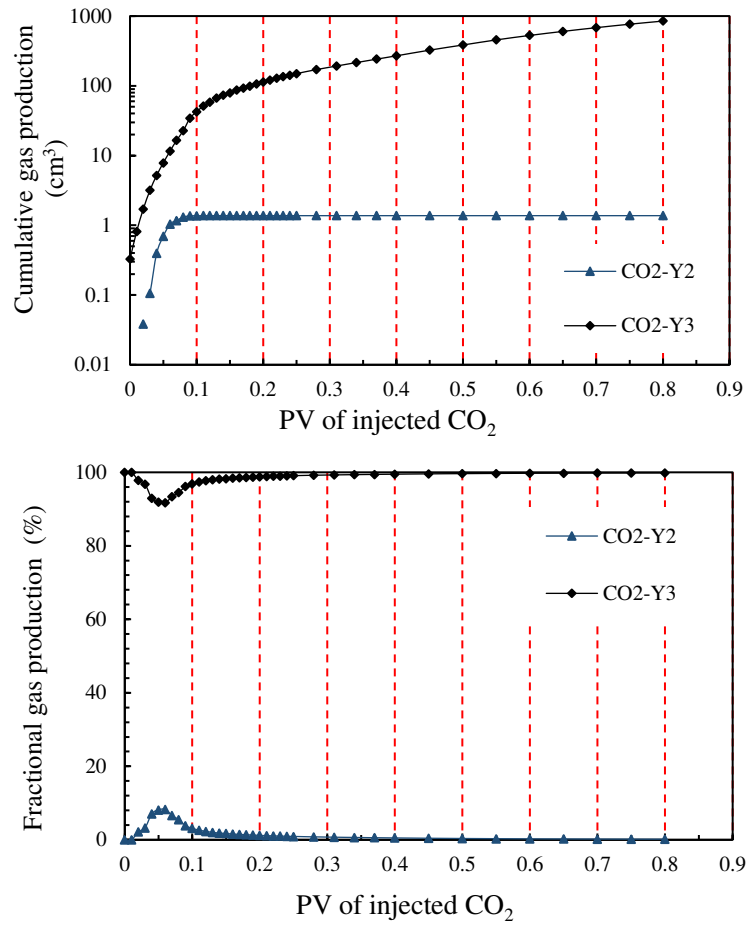


Figure 8. Produced gas of each core during CO₂ flooding.

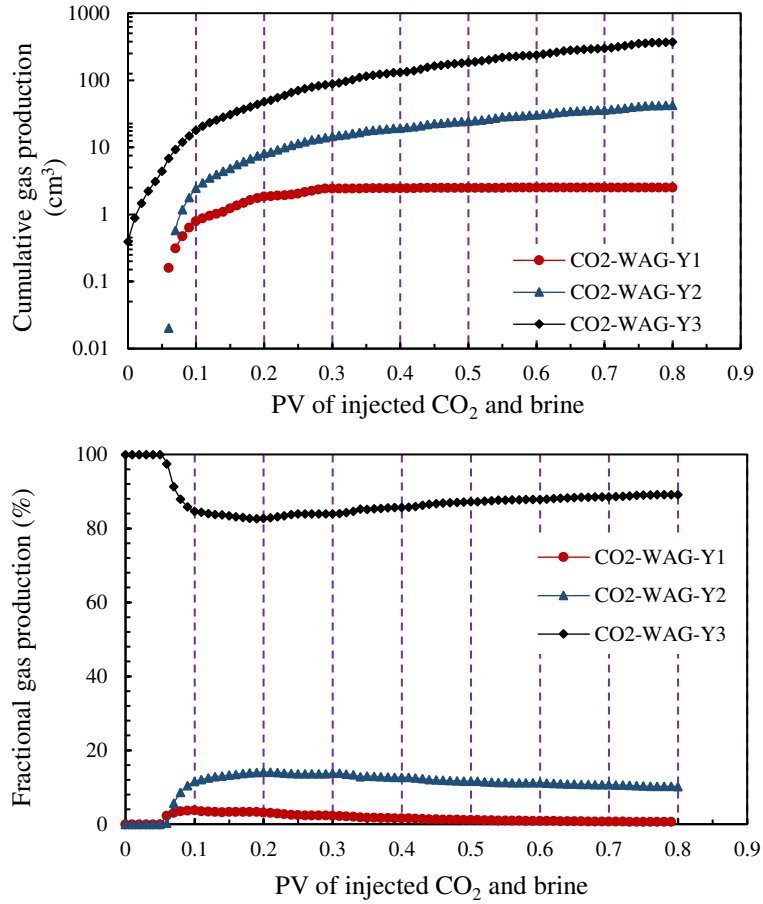


Figure 9. Produced gas of each core during CO₂-WAG flooding.

Table 7. Collected liquid (oil + brine) of each core during flooding.

	PV	Liquid volume (ml)		
		Y1	Y2	Y3
CO ₂ -WAG	0.3	-	-	1.3
	0.8	-	0.4	2.6
CO ₂	0.3	-	-	1.1
	0.8	-	-	1.2

During CO₂ flooding, the difference in the cumulative volume of gas production of each layer of the multilayer system is large, and CO₂ BT exacerbates this difference [20]. However, the difference is smaller in the CO₂-WAG flooding process, and the effect of CO₂ BT on this difference is weaker than that during CO₂ flooding. These observations can be attributed to the fact that WAG flooding effectively reduces the difference in capillary resistance in layers with different permeability, even after the CO₂ BT [18]. In addition, high pressures increase the contribution of liquid and gas production of medium and low permeability layers compared to that during CO₂ flooding.

The variations of components and asphalt in the produced oil are shown in Figure 10 and Table 8, as the volume of oil collected from medium and low permeability cores was small, only the produced oil samples collected from high permeability cores were tested.

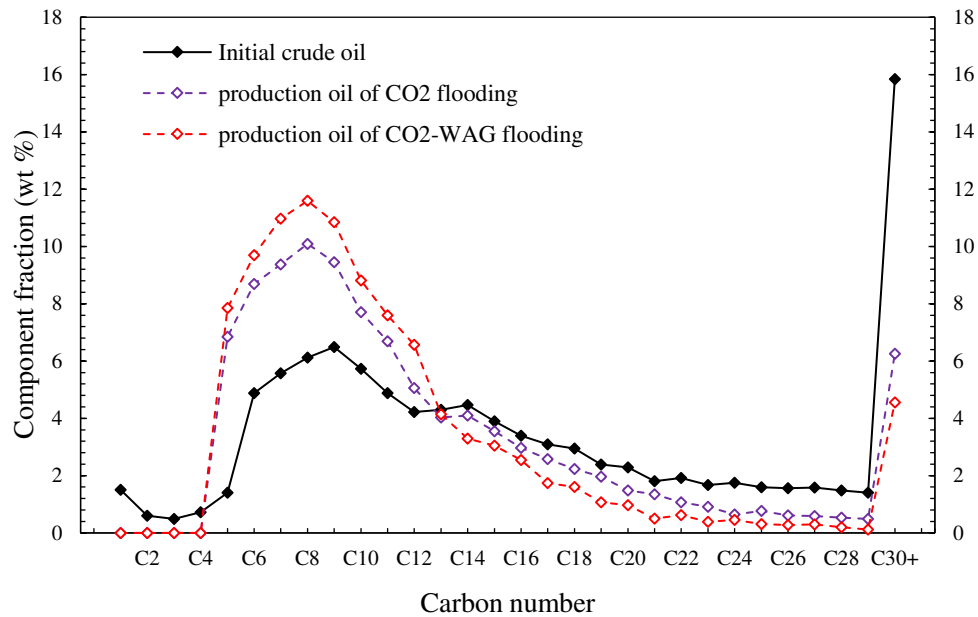


Figure 10. Components of produced oil of the high permeability cores.

Table 8. Asphalt in produced oil of the high permeability cores.

Core number	Asphaltene in oil (wt %)	
	Initial oil	produced oil
Y3-1(CO ₂ -WAG)	1.32	0.38
Y3-2(CO ₂)	1.32	0.47

The proportion of light components in the produced oil is higher than that of the original crude oil sample, especially in core Y3-1 after CO₂-WAG flooding. The light-hydrocarbon extraction effect of CO₂ on crude oil in cores during CO₂-WAG flooding is stronger than that during CO₂ flooding. Consequently, the produced oil from Y3-1 has lower asphaltene content, and more asphaltene is retained in the core, which means that the asphaltene precipitation caused by the dissolution of CO₂ into the crude oil is more serious. This is attributed to the higher pressures in core Y3-1 CO₂-WAG flooding. Higher pressures result in higher CO₂ concentrations in crude oil during CO₂-WAG flooding, which is the key factor in controlling the deposition of asphaltene from crude oil [33].

Residual oil distribution and oil recovery

The distribution and proportion of residual oil in all cores after the flooding experiments are shown in Figure 11 and Table 9. The oil production from each core based on the distribution of residual oil is shown in Figure 12.

The residual oil of the multilayer system is mainly distributed in the medium and low permeability cores after CO₂ flooding, and there is also a relatively small proportion of residual oil in the small pores of the high permeability core. Correspondingly, the high permeability core has the highest oil RF and contribution percentage fraction (CPF, the fraction of oil produced by each core expressed as a percentage of total system oil production) of oil production, and the oil recovery of the multilayer system was determined by the high permeability core. The oil RF of the entire system was very low, 27.64%. This finding is caused mainly by the heterogeneity of the reservoir and the fingering effect in the high permeability core, which results from differences in capillary resistance in different cores and leads to premature CO₂ BT ^[46]. Hence, a large amount of CO₂ injected into the multilayer system flowed out through the CO₂ channel in the high-permeability core, and in doing so did not contribute to the production of hydrocarbons and is consequently associated with a low efficiency of CO₂ flooding.

However, for CO₂-WAG flooding, the residual oil was less than that in the corresponding core after CO₂ flooding, and the difference in the proportion of residual oil between the high permeability core and the other two cores was also smaller. Therefore, medium and low permeability cores had relatively higher oil RF and CPF of oil production than CO₂ flooding, as well as the higher oil RF of the entire system, 44.49%. It is worth noting that the recovery coefficients of high, medium and low permeability cores after CO₂-WAG flooding were 22.26%, 16.45% and 6.37% higher than that after CO₂ flooding, respectively, oil displacement efficiency of CO₂-WAG showed the greatest improvement in high permeability core. Furthermore, for the cores with same permeability, during CO₂-WAG flooding the core had the lower size cut-off of pores in which oil can be driven out, and the high permeability core had the lowest cut-off point among the six cores. In high permeability core, due to higher pressure and suppression of gas channel by the way of CO₂-WAG, the injected fluid can enter or dissolve in the crude oil in the smaller pores, increasing the sweep volume and oil displacement efficiency in the cores. In addition, a part of the fluid enters and the medium and low permeability cores under a higher differential pressure, the oil displacement effect of the injected fluid on these cores is also improved ^[13, 18]. In general, CO₂-WAG flooding not only improves the oil displacement effect of each layer, especially the high permeability layer, but also weakens the impact of multilayer system heterogeneity on the overall system oil recovery performance.

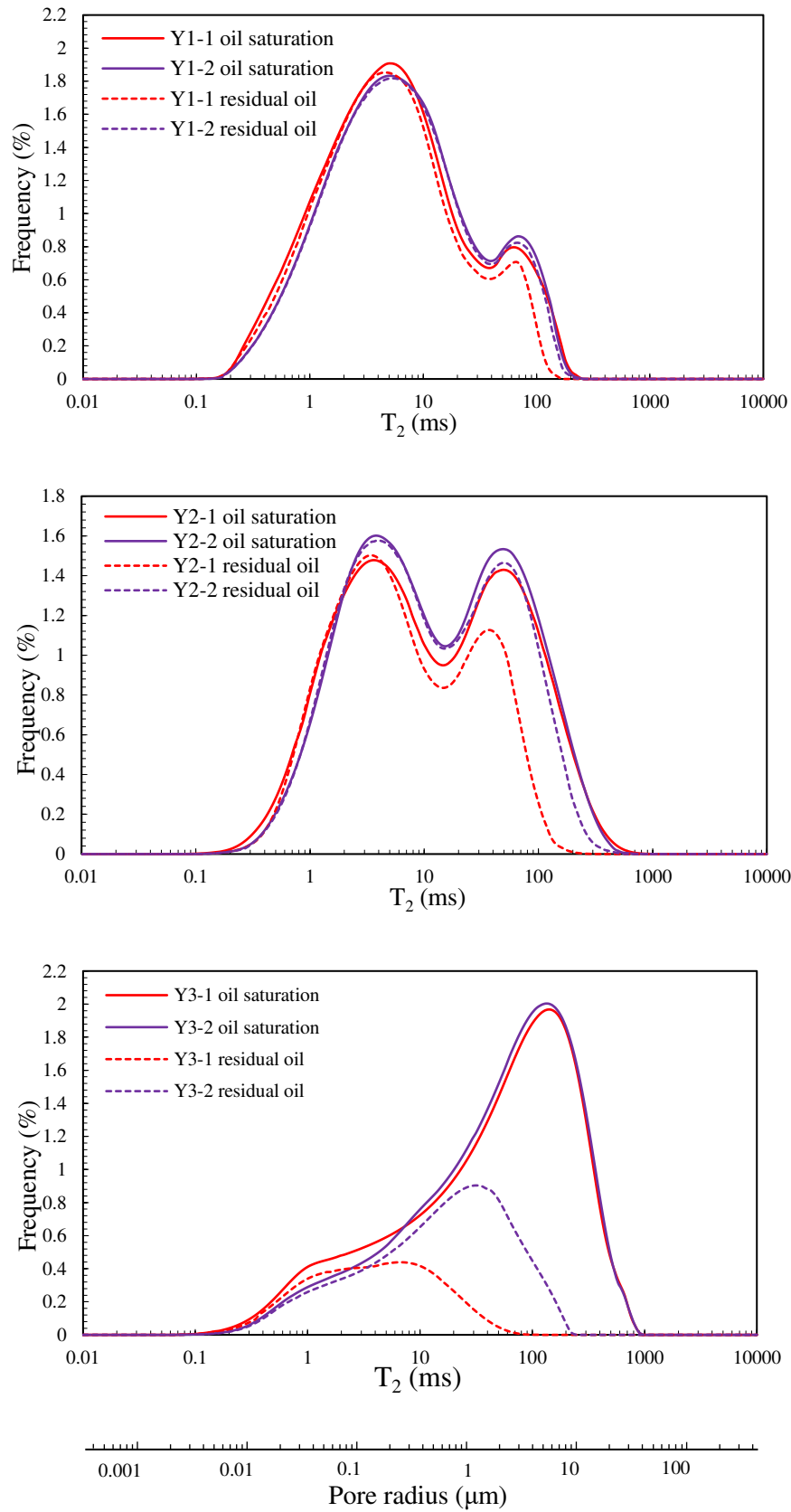


Figure 11. NMR T_2 spectrum of oil distribution in cores after experiments.

Table 9. The proportion of residual oil in each core after the flooding experiments.

	Proportion of residual oil (%)			
	Y1	Y2	Y3	entire system
CO ₂ -WAG	91.66	77.78	23.14	55.51
CO ₂	98.03	94.22	45.40	72.36

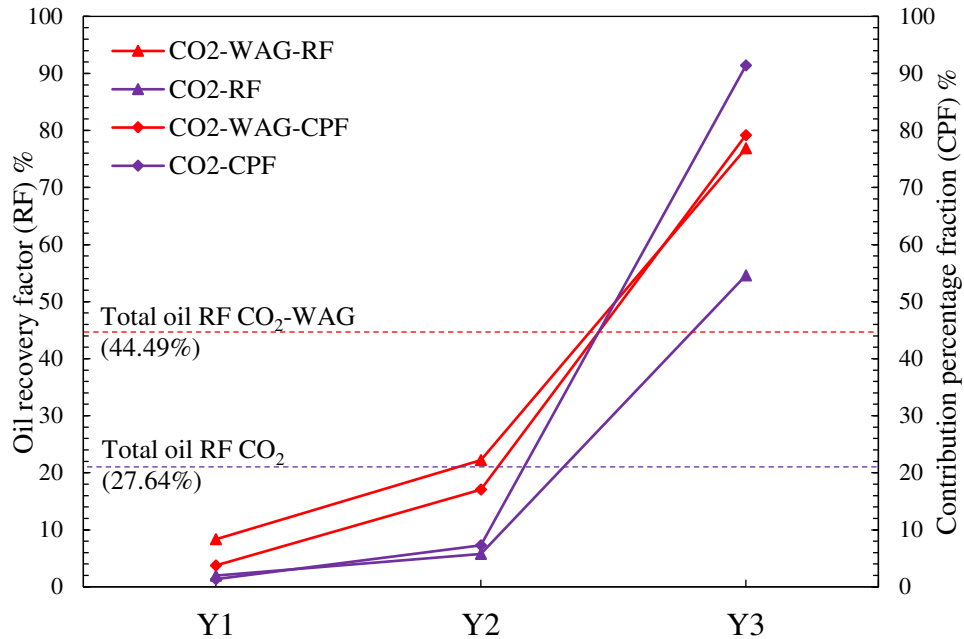


Figure 12. The oil production of each core calculated based on distribution of residual oil after experiments.

Permeability damage

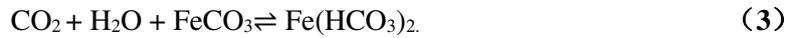
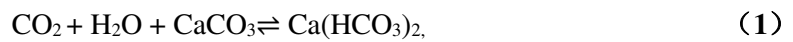
The changes in permeability and porosity of the cores due to both types of core flooding can be obtained by comparing permeability porosity measurements before and after the flooding experiments, as shown in Table 10. The permeability of all cores showed a decline, but to different extents. In the same group of flooding experiments, the trend of permeability decline was found to depend upon the initial permeability of the core; the greater the initial permeability of the core, the greater the decrease of permeability. In all cases WAG flooding led to a greater decrease in permeability than simple CO₂ flooding. The decrease in porosity was much less dramatic for all cores and flooding techniques, varying in size from 1% to 3.5%, as expected for the scalar petrophysical property.

Table 10. Permeability and porosity of cores before and after flooding experiments.

	Core number	k_b (mD)	k_a (mD)	$1-k_a/k_b$ (%)	ϕ_b (%)	ϕ_a (%)	$1-\phi_a/\phi_b$ (%)
CO ₂ -WAG	Y1-1	0.58	0.54	6.87	10.61	10.26	3.30
	Y2-1	6.78	5.64	16.81	16.69	16.21	2.88
	Y3-1	63.6	44.9	29.40	19.98	19.21	3.85
CO ₂	Y1-2	0.59	0.58	1.85	10.68	10.57	1.03
	Y2-2	6.92	6.48	6.36	16.87	16.42	2.67
	Y3-2	64.1	53.8	16.07	19.85	19.43	2.12

k_b , core permeability before flooding k_a , core permeability after flooding $1-k_a/k_b$, permeability decline ϕ_b , core porosity before flooding ϕ_a , core porosity after flooding $1-\phi_a/\phi_b$, porosity decline

The significant decreases in permeability and slight decreases in porosity of cores are attributed to changes in the microstructure of pores and throats in rocks caused by migration of particles due to organic deposition and CO₂-brine-rock interaction [23-24]. When CO₂ is injected into cores and the concentration in the crude oil reaches 19.6 mol% (in this work), the asphaltenes begin to precipitate from the crude oil and aggregate to become asphaltene particles. The size of the particles produced by asphaltene flocculation is reported to be distributed at 0.1-10 μm [47,48]. These asphaltene particles are adsorbed on the pore wall of the rock or are captured at the throats during the process of migration with fluid in cores [26,49-51]. Moreover, CO₂-brine-rock interactions lead to dissolution of carbonate minerals and destruction of clay mineral structure in rocks. Metal carbonate precipitation occurs due to changes in pH and the concentration of metal ions (i.e., Ca²⁺, Mg²⁺, Fe²⁺) in the fluid of the cores (Equations 1-3), and additional clay particles are released caused by structural instability [29-30]. It has been reported that low-permeability sandstones undergo CO₂ flooding and CO₂-WAG flooding, and the concentration of suspended solid particles in the produced brine ranges from 0 to 6720 mg/L with an average size of 1049.7 nm [24]. Three of the most common carbonate minerals formed in pores and capable of blocking pore throats are given by the equations



Since the size distribution of particles overlaps with the pore size distribution of rocks, when the asphaltene particles, metal hydrogen carbonate particles and clay particles migrate in rocks, particles that are much smaller in size than the pore throats are likely to be adsorbed to the pore surfaces, particles that are large in size than the pore throats are likely to be trapped at the throats [24]. The migration of these particles cause blockages in the pores and throats of the rocks during the flooding process, as shown in Figure 13. Blockage or partial blockage of flow pathways may have little effect on rock porosity but can reduce permeability significantly because permeability is a vector petrophysical property that is highly sensitive to the connectedness of the pore microstructure [52].

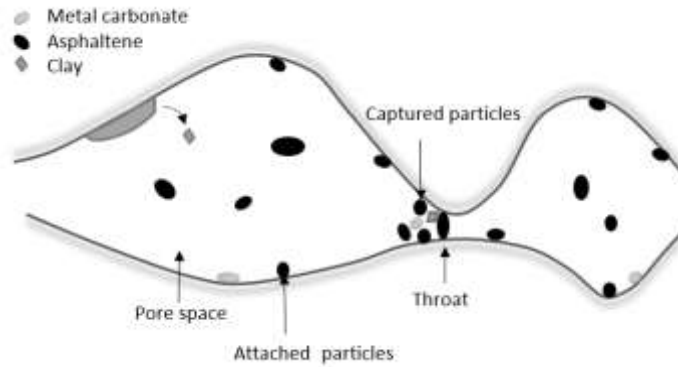


Figure 13. Schematic diagram of the pore spaces and throats blocked by particles.

Since the cores with different permeability were flooded in parallel, the volume of fluid injected into the cores with high permeability was larger than that of the cores with lower permeability, which means that the crude oil and the minerals in the cores are in contact with more injected fluids and the interactions are more complete, producing more organic and inorganic precipitates and movable clay particles. Furthermore, as a larger volume of fluid flows through the core, which means a more adequate and more powerful particle migration, the particles carried by the fluid have a higher probability of being captured at the throats, enhancing the filtration of particles in the fluid by the porous medium ^[53-54]. Consequently, more blockages at throats result in a greater decrease in permeability for those cores with large permeability. However, those cores with lower permeability used in this work have smaller average sizes of pores and throats, and the changes in permeability are more sensitive to blockages caused by precipitation and clay particles. The ratios of the decrease in permeability of three cores were 1:3.4:8.7 and 1:2.4:4.3 for CO₂ and WAG flooding, respectively (Figure 14), which are both much smaller than the ratios of the initial permeability (1:11.6:108). In other words the high permeability initial material had a permeability 108 times higher than the low permeability initial material, which means much more serious blockage in the pores of high permeability core due to the much larger volume of fluid flowing through during flooding, but once CO₂ flooding have been completed the high permeability material only had a permeability decline 8.7 times larger than the low permeability material, and after WAG flooding the permeability decline of high permeability material was 4.3 times larger than that of the low permeability material. The effect of difference in volume of injected fluid caused by the initial permeability on the difference in permeability decrease between different cores are weakened due to the difference in pore throat distribution.

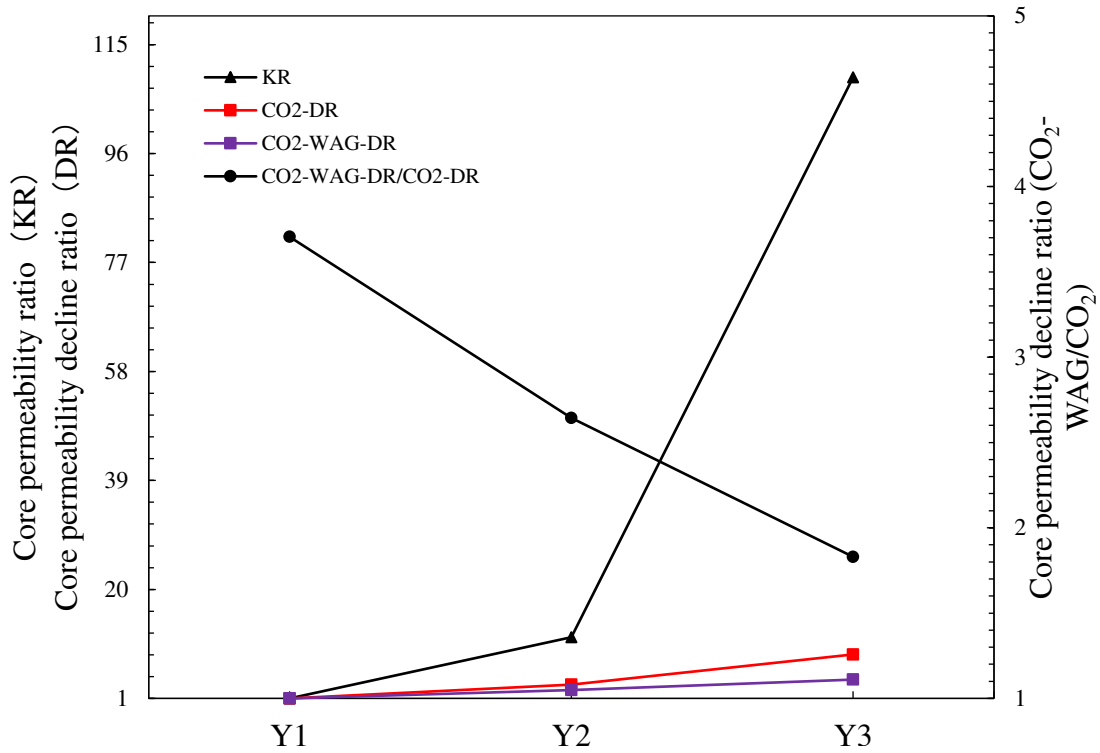


Figure 14. Permeability decline ratio and initial permeability ratio between cores. Symbols: KR, ratios of initial permeability, $KR_{Y1}:KR_{Y2}:KR_{Y3}$. DR, ratios of permeability decline, KR_{Y1} decline: KR_{Y2} decline: KR_{Y1} decline CO_2 -WAG-DR/ CO_2 -DR, the ratios of the permeability decline after CO_2 -WAG flooding to the permeability decline after CO_2 flooding, KR_{Y1-1} decline: KR_{Y1-2} decline; KR_{Y2-1} decline: KR_{Y2-2} decline; KR_{Y1-3} decline: KR_{Y3-2} decline

In addition, the permeability decrease of cores after CO_2 flooding was less than that of the corresponding core after CO_2 -WAG flooding. The injection of CO_2 -WAG combines the improved volumetric sweep efficiency of water flooding and the enhanced microscopic displacement efficiency of CO_2 flooding. The injected CO_2 and crude oil become miscible, making crude oil easy to be displaced. The injected brine can quickly increase and maintain the pressure (above the MMP) so as to effectively control the mobility of the injected CO_2 by reducing its relative permeability, which also strengthens the dissolution of CO_2 in crude oil [38, 42]. The effects of these displacement characteristics on the generation and migration of organic and inorganic particles can be attributed to three factors during CO_2 -WAG flooding, higher injection pressure, larger sweep volume of the injected fluid and stronger power of particle migration during CO_2 -WAG flooding. At higher pressures, CO_2 concentration dissolved in oil or brine in the cores is higher, crude oil dissolved with more CO_2 causes more asphaltenes to deposit, brine dissolved with more CO_2 makes CO_2 -brine-rock interactions more complete, resulting in more organic and inorganic precipitation in pores. The larger sweep volume means that production of movable organic and inorganic particles in more numerous and smaller pores and pore throats. Greater displacement power due to higher pressure, higher viscosity of water (compared with CO_2) and lower viscosity of crude oil (dissolved more CO_2) make the particles more

fully migrated with the fluid, and the pressure fluctuation generated during the switch of CO₂-brine injection exacerbates the migration and blockage of particles. Furthermore, the difference in the permeability decreases of the three cores after WAG flooding is smaller than that after CO₂ flooding, which can be attributed to relatively more CO₂ injected into the cores with lower permeability during CO₂-WAG flooding. This reason also leads to a large difference in permeability decrease between low permeability cores (Y1-1,Y1-2) after different flooding methods (Figure 14), but the difference in permeability decrease caused by flooding methods is smaller in high permeability cores (Y3-1,Y3-2). This is because in both flooding methods, the cores with high permeability are always the main flow channel for the injected fluid relative to the cores with lower permeability, and CO₂-WAG only improves this difference.

Figure 15 shows that the permeability decline due to asphaltene precipitation during the CO₂ flooding is dominant, namely around 95%. Since the connate water is distributed in the smallest pores or covers the surface of the minerals in the form of a water film [37], the injected CO₂ finds it difficult to come into contact with the brine and minerals, and CO₂-brine-rock interactions have little effect on the permeability decline. In CO₂-WAG flooding, the permeability decline caused by the CO₂-brine-rock interactions is significantly higher than that in CO₂ flooding, and as the initial permeability increases, the ratio of the permeability decline caused by asphaltene precipitation to the total permeability decline decreases. This is because more crude oil is displaced from the cores, especially from the cores with high permeability, and the pervasive distribution of brine and CO₂ during the flooding process making brine and CO₂ more likely to be in contact with minerals, enhancing the CO₂-brine-rock interactions.

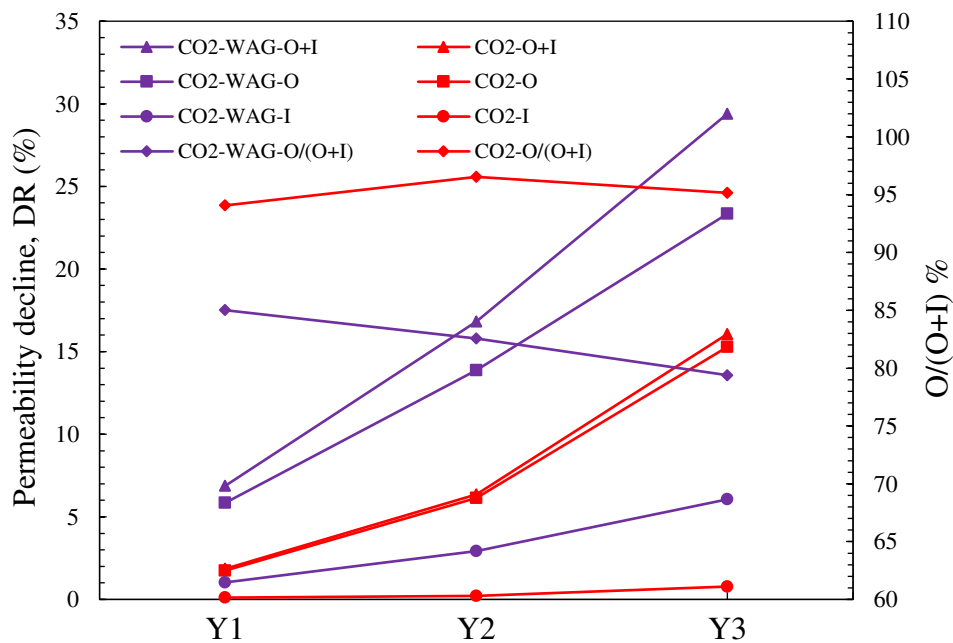


Figure 15. Permeability decline of cores after flooding experiments. Symbols: O, permeability decline due to organic precipitation (asphaltene); I, permeability decline due to inorganic interactions.

However, despite this, the absolute value of permeability decline caused by asphaltene precipitation in all cores after CO₂-WAG flooding is still higher than that after CO₂ flooding. Besides the higher pressure, **the distribution of fluid during flooding is also a key factor**. As the non-wetting phase CO₂ exists mainly in large pores, and injected CO₂ does not come into contact with the crude oil in the smaller pores, and hence does not cause asphaltene precipitation in these pores during CO₂ flooding. After CO₂ BT in the high permeability core, most of the CO₂ flows through the gas channel(s) which have formed from the input face of the core to the output face. While flowing through these channels the CO₂ interact with little oil and so the probability of asphaltene precipitation is generally small, and asphaltene precipitation in small pores away from the main gas channels will not occur. In CO₂-WAG flooding there is an inhibitory effect on the formation of gas channels even after CO₂ BT, which results in a greater opportunity for CO₂ to find itself in contact with crude oil in both the larger and smaller pores in the rock, resulting in asphaltene precipitation in a wider range of pores.

In summary, damage of organic precipitation and inorganic interaction to core permeability are controlled by pore size distribution, displacement fluid volume and fluid distribution during flooding, and the three factors are related to initial permeability and flooding methods.

Conclusion

In this paper, the MMP of the CO₂-crude oil system and petrophysical properties of two groups of cores were measured. Core flooding experiments using CO₂ and CO₂-WAG schemes were carried out on multilayer/multi permeability system with very similar physical properties under miscible conditions. After CO₂ and CO₂-WAG flooding, the fluid production and residual oil distribution for each layer in the multilayer system were evaluated, and the damage to the permeability of the organic and inorganic interactions of CO₂-oil-brine-rock was compared. Based on the experimental results, the following conclusions can be drawn.

During CO₂ flooding, the average injection pressure is lower, and only the high permeability layer has obvious CO₂ BT. The use of CO₂-WAG can delay the occurrences of CO₂ BT, and more asphaltene is precipitated from the crude oil in the rock during CO₂-WAG flooding, but the extraction effect of CO₂ on crude oil is weaker than that during CO₂ flooding in the high permeability layer.

Due to different capillary resistance, the oil and gas production of the whole system are almost exclusively from the high-permeability layer, with the medium and low permeability layer having extremely low oil RFs after CO₂ flooding. The CO₂-WAG core floods showed a higher oil

displacement efficiency and an ability to reduce the impact of interlayer heterogeneity, improving the contribution rate of oil and gas production in medium and low permeability layers.

Since the high-permeability layer acts as the main CO₂ channel, only the permeability of the high-permeability layer decreases clearly after CO₂ flooding, and the permeability reduction is mainly caused by asphaltene precipitation. The CO₂-WAG core flooding can effectively control the gas channel in the high permeability layer, the permeability of each layer after CO₂-WAG flooding decreases more than that in the corresponding layer after CO₂ flooding. Moreover, the decrease in permeability caused by CO₂-brine-rock interactions cannot be ignored, which is more obvious in the layer with high permeability.

Overall, it is possible to say that CO₂-WAG flooding has advantages in crude oil recovery performance in heterogeneous multilayer systems, but requires higher injection pressures and results in more severe damage to reservoir permeability than CO₂ flooding.

Acknowledgments

Thanks are given to the teams at Beijing RIPED. This research is supported by National Natural Science Foundation of China, “Study on the physical basis of seepage in ultra-deep clastic reservoirs” (51774300), and “Key technologies for CO₂ flooding and storage” of the 13th Five-Year National Major Science and Technology Project (2016ZX05016006-004).

References

- (1) Ghedan, S. Global laboratory experience of CO₂-EOR flooding. *SPE/EAGE reservoir characterization & simulation conference*, 2009.
- (2) Ampomah, W., Balch, R., Cather, M., Rose-Coss, D., Dai, Z., Heath, J., Dewers, T. and Mozley, P. Evaluation of CO₂ storage mechanisms in CO₂ enhanced oil recovery sites: Application to Morrow sandstone reservoir. *Energy & Fuels*, 2016, 30(10), 8545-8555.
- (3) Barclay, T. H., Srikanta, M. New correlations for CO₂-Oil solubility and viscosity reduction for light oils. *Journal of Petroleum Exploration and Production Technology* 2016, 6(4), 815-823.
- (4) Or, C., Sasaki, K., Sugai, Y., Nakano, M. & Imai, M. Swelling and viscosity reduction of heavy oil by CO₂-gas foaming in immiscible condition. *SPE Reservoir Evaluation & Engineering*, 2016, 19(02), 294-304.
- (5) Riazi, M., Mehran, S., Mahmoud, J. Experimental study of pore-scale mechanisms of carbonated water injection. *Transport in porous media*, 2011, 86(1), 73-86.
- (6) Abedini, A., Farshid, T. On the CO₂ storage potential of cyclic CO₂ injection process for enhanced oil recovery. *Fuel*, 2014, 124, 14-27.
- (7) Jia, B., Jyun-Syung, T., Reza, B. A review of the current progress of CO₂ injection EOR and carbon storage in shale oil reservoirs. *Fuel*, 2019, 236, 404-427.
- (8) Ren, B., Ian, D. Modelling oil saturation evolution in residual oil zones: Implications for CO₂ EOR and sequestration. *Journal of Petroleum Science and Engineering* 2019, 177, 528-539.
- (9) Zhang, K., Gu, Y. Two new quantitative technical criteria for determining the minimum miscibility pressures (MMPs) from the vanishing interfacial tension (VIT) technique. *Fuel*, 2016, 184, 136-144.

- (10) Ghorbani, M., Momeni, A., Safavi, S. and Gandomkar, A. Modified vanishing interfacial tension (VIT) test for CO₂–oil minimum miscibility pressure (MMP) measurement. *Journal of Natural Gas Science and Engineering*, 2014, 20, 92-98.
- (11) Hawthorne, S. B., Miller, D. J., Jin, L., & Gorecki, C. D. Rapid and simple capillary-rise/vanishing interfacial tension method to determine crude oil minimum miscibility pressure: pure and mixed CO₂, methane, and ethane. *Energy & Fuels*, 2016, 30(8), 6365-6372.
- (12) Qian, K., Yang, S., Dou, H., Wang, Q., Wang, L. and Huang, Y. Experimental investigation on microscopic residual oil distribution during CO₂ Huff-and-Puff process in tight oil reservoirs. *Energies*, 2018, 11(10), 2843.
- (13) Han, L., Gu, Y. Optimization of miscible CO₂ water-alternating-gas injection in the Bakken formation. *Energy & Fuels*, 2014, 28(11), 6811-6819.
- (14) Teklu, T.W., Alameri, W., Graves, R.M., Kazemi, H. and AlSumaiti, A.M. Low-salinity water-alternating-CO₂ EOR. *Journal of Petroleum Science and Engineering*, 2016, 142, 101-118.
- (15) Seyyedi, M., Mehran, S. Assessing the Feasibility of Improving the Performance of CO₂ and CO₂–WAG Injection Scenarios by CWI. *Industrial & Engineering Chemistry Research*, 2018, 57(34), 11617-11624.
- (16) Zhou, X., Yuan, Q., Zhang, Y., Wang, H., Zeng, F. and Zhang, L. Performance evaluation of CO₂ flooding process in tight oil reservoir via experimental and numerical simulation studies. *Fuel*, 2019, 236, 730-746.
- (17) Wang, S., Kadhum, M.J., Chen, C., Shiau, B. and Harwell, J.H. Development of in situ CO₂ generation formulations for enhanced oil recovery. *Energy & fuels* 2017, 31(12), 13475-13486.
- (18) Jaber, A.K., Awang, M.B. and Lenn, C.P. Box-Behnken design for assessment proxy model of miscible CO₂-WAG in heterogeneous clastic reservoir. *Journal of Natural Gas Science and Engineering*, 2017, 40, 236-248.
- (19) Chen, B., Albert, C. R. CO₂ water-alternating-gas injection for enhanced oil recovery: Optimal well controls and half-cycle lengths. *Computers & Chemical Engineering* 2018, 113, 44-56.
- (20) Han, J., Lee, M., Lee, W., Lee, Y. and Sung, W. Effect of gravity segregation on CO₂ sequestration and oil production during CO₂ flooding. *Applied energy*, 2016, 161, 85-91.
- (21) Hamidi, H., Haddad, A.S., Mohammadian, E., Rafati, R., Azdarpour, A., Ghahri, P., Ombewa, P., Neuert, T. and Zink, A. Ultrasound-assisted CO₂ flooding to improve oil recovery. *Ultrasonics sonochemistry*, 2017, 35, 243-250.
- (22) Lei, H., Yang, S., Zu, L., Wang, Z. and Li, Y. Oil recovery performance and CO₂ storage potential of CO₂ water-alternating-gas injection after continuous CO₂ injection in a multilayer formation. *Energy & Fuels*, 2016, 30(11), 8922-8931.
- (23) Yu, M., Liu, L., Yang, S., Yu, Z., Li, S., Yang, Y. and Shi, X. Experimental identification of CO₂–oil–brine–rock interactions: Implications for CO₂ sequestration after termination of a CO₂-EOR project. *Applied geochemistry*, 2016, 75, 137-151.
- (24) Wang, Z., Yang, S., Lei, H., Yang, M., Li, L. and Yang, S. Oil recovery performance and permeability reduction mechanisms in miscible CO₂ water-alternative-gas (WAG) injection after continuous CO₂ injection: An experimental investigation and modeling approach. *Journal of Petroleum Science and Engineering*, 2017, 150, 376-385.
- (25) Lei, H., Yang, S., Qian, K., Chen, Y., Li, Y. and Ma, Q. Experimental investigation and application of the asphaltene precipitation envelope. *Energy & Fuels*, 2015, 29(11), 6920-6927.
- (26) Cho, J., Kim, T.H., Chang, N. and Lee, K.S. Effects of asphaltene deposition-derived formation damage on three-phase hysteretic models for prediction of coupled CO₂ enhanced oil recovery and storage performance. *Journal of Petroleum Science and Engineering*, 2019, 172, 988-997.
- (27) Qian, K., Yang, S., Dou, H.E., Pang, J. and Huang, Y. Formation damage due to asphaltene precipitation during CO₂ flooding processes with NMR technique. *Oil & Gas Science and Technology–Revue d'IFP Energies nouvelles*, 2019, 74, 11.

- (28) Wang, C., Li, T., Gao, H., Zhao, J. and Gao, Y. Quantitative study on the blockage degree of pores due to asphaltene precipitation in low-permeability reservoirs with NMR technique. *Journal of Petroleum Science and Engineering*, 2018, 163, 703-711.
- (29) Yu, Z., Liu, L., Yang, S., Li, S., & Yang, Y. An experimental study of CO₂-brine-rock interaction at in situ pressure-temperature reservoir conditions. *Chemical Geology*, 2012, 326, 88-101.
- (30) Wang, Q., Yang, S., Han, H., Wang, L., Qian, K. and Pang, J. Experimental Investigation on the Effects of CO₂ Displacement Methods on Petrophysical Property Changes of Ultra-Low Permeability Sandstone Reservoirs near Injection Wells. *Energies*, 2019, 12(2), 327.
- (31) Gaus, I. Role and impact of CO₂-rock interactions during CO₂ storage in sedimentary rocks. *International Journal of Greenhouse Gas Control*, 2010, 4, 73-89.
- (32) Bikkina, P., Wan, J., Kim, Y., Kneafsey, T.J. and Tokunaga, T.K. Influence of wettability and permeability heterogeneity on miscible CO₂ flooding efficiency. *Fuel*, 2016, 166, 219-226.
- (33) Mahzari, P., Tsohis, P., Sohrabi, M., Enezi, S., Yousef, A.A. and Eidan, A.A. Carbonated water injection under reservoir conditions; in-situ WAG-type EOR. *Fuel*, 2018, 217, 285-296.
- (34) Afzali, S., Rezaei, N., & Zendehboudi, S. A comprehensive review on enhanced oil recovery by water alternating gas (WAG) injection. *Fuel*, 2018, 227, 218-246.
- (35) Xiao, P., Yang, Z., Wang, X., Xiao, H. and Wang, X. Experimental investigation on CO₂ injection in the Daqing extra/ultra-low permeability reservoir. *Journal of Petroleum Science and Engineering*, 2017, 149, 765-771.
- (36) Wang, S., Chen, S., Li, Z. Characterization of produced and residual oils in the CO₂ flooding process. *Energy & Fuels*, 2015, 30(1), 54-62.
- (37) Xiao, P., Lv, C., Wang, R., Cui, M., Xu, Q., Hu, Q. and Hu, W. Laboratory study heterogeneity impact on microscopic residual oil distribution in tight sandstone cores during CO₂ immiscible flooding. *Energy Sources, Part A: Recovery, Utilization, and Environmental Effects*, 2019, 1-11.
- (38) Ahmadi, Y., Eshraghi, S.E., Bahrami, P., Hasanbeygi, M., Kazemzadeh, Y. and Vahedian, A. Comprehensive Water-Alternating-Gas (WAG) injection study to evaluate the most effective method based on heavy oil recovery and asphaltene precipitation tests. *Journal of Petroleum Science and Engineering*, 2015, 133, 123-129.
- (39) Zanganeh, P., Dashti, H. & Ayatollahi, S. Visual investigation and modeling of asphaltene precipitation and deposition during CO₂ miscible injection into oil reservoirs. *Fuel*, 2015, 160, 132-139.
- (40) Cao, M., Gu, Y. Oil recovery mechanisms and asphaltene precipitation phenomenon in immiscible and miscible CO₂ flooding processes. *Fuel*, 2013, 109, 157-166.
- (41) Abedini, A., Torabi, F. Oil recovery performance of immiscible and miscible CO₂ huff-and-puff processes. *Energy & Fuels*, 2014, 28(2), 774-784.
- (42) Chen, J., Li, T., Wu, S. Influence of pressure and CO₂ content on the asphaltene precipitation and oil recovery during CO₂ flooding. *Petroleum Science and Technology*, 2018, 36(8), 577-582.
- (43) Saeedi, A., Delle Piane, C., Esteban, L. and Xie, Q. Flood characteristic and fluid rock interactions of a supercritical CO₂, brine, rock system: South West Hub, Western Australia. *International Journal of Greenhouse Gas Control*, 2016, 54, 309-321.
- (44) Zou, Y., Li, S., Ma, X., Zhang, S., Li, N. and Chen, M. Effects of CO₂-brine-rock interaction on porosity/permeability and mechanical properties during supercritical-CO₂ fracturing in shale reservoirs. *Journal of Natural Gas Science and Engineering*, 2018, 49, 157-168.
- (45) Fang, T., Zhang, L., Liu, N., Zhang, L., Wang, W., Yu, L., Li, C. and Lei, Y. Quantitative characterization of pore structure of the Carboniferous-Permian tight sandstone gas reservoirs in eastern Linqing depression by using NMR technique. *Petroleum Research*, 2018, 3(2), 110-123.

- (46) Alhamdan, M.R., Cinar, Y., Suicmez, V.S. and Dindoruk, B. Experimental and numerical study of compositional two-phase displacements in layered porous media. *Journal of Petroleum Science and Engineering*, 2012, 98, 107-121.
- (47) Mansur, C.R., de Melo, A.R. and Lucas, E.F. Determination of asphaltene particle size: influence of flocculant, additive, and temperature. *Energy & Fuels*, 2012, 26 (8), pp.4988-4994.
- (48) Najafi, I., Mousavi, S.M.R., Ghazanfari, M.H., Ghotbi, C., Ramazani, A., Kharrat, R. and Amani, M. Quantifying the role of ultrasonic wave radiation on kinetics of asphaltene aggregation in a toluene-pentane mixture. *Petroleum Science and Technology*, 2011, 29(9), pp.966-974.
- (49) Sim, S. S. K., Okatsu, K., Takabayashi, K. & Fisher, D. B. Asphaltene-induced formation damage: effect of asphaltene particle size and core permeability. *SPE Annual Technical Conference and Exhibition. Society of Petroleum Engineers*, 2005.
- (50) Jafari Behbahani, T., Ghotbi, C., Taghikhani, V. and Shahrabadi, A. Investigation on asphaltene deposition mechanisms during CO₂ flooding processes in porous media: a novel experimental study and a modified model based on multilayer theory for asphaltene adsorption. *Energy & Fuels*, 2012, 26(8), 5080-5091.
- (51) Fakher, S., Abdulmohsin, I. Investigating and Mitigating Asphaltene Precipitation and Deposition in Low Permeability Oil Reservoirs during Carbon Dioxide Flooding to Increase Oil Recovery. *SPE Annual Caspian Technical Conference and Exhibition. Society of Petroleum Engineers*, 2018.
- (52) Glover, P.W. and Walker, E. Grain-size to effective pore-size transformation derived from electrokinetic theory. *Geophysics*, 2008, 74(1), pp.E17-E29
- (53) Mendoza de la Cruz, J.L., Argüelles-Vivas, F.J., Matías-Pérez, V., Durán-Valencia, C.D.L.A. and López-Ramírez, S. Asphaltene-induced precipitation and deposition during pressure depletion on a porous medium: an experimental investigation and modeling approach. *Energy & Fuels*, 2019, 23(11), 5611-5625.
- (54) Monteagudo, J. E., Rajagopal, K. & Lage, P. L. Simulating oil flow in porous media under asphaltene deposition. *Chemical Engineering Science*, 2012, 57(3), 323-337.